Major Classification: Physical Sciences

Minor Classification: Applied Physical Sciences

**On the Evaporation of Ammonium Sulfate Solution**

Walter S. Drisdell[1,2], Richard J. Saykally[1,2], and Ronald C. Cohen[1,3]*

Department of Chemistry, University of California, Berkeley, California 94720-1460

Chemical Sciences Division, Lawrence Berkeley National Laboratory, Berkeley, California 94720-8176

Department of Earth and Planetary Science, University of California, Berkeley, California 94720-4767

*To whom correspondence should be addressed

E-mail: rccohen@berkeley.edu

Fax: (510) 643-2156

Telephone: (510) 642-2735

Manuscript Information:

Pages: 20 Figures: 2 Tables: 0

Abbreviations: MD, Molecular Dynamics; CPMD, Car-Parrinello Molecular Dynamics

**Abstract:**

Aqueous evaporation and condensation kinetics are poorly understood and uncertainties in their rates affect predictions of cloud behavior and therefore climate. We measured the cooling rate of 3M ammonium sulfate droplets undergoing free evaporation via Raman thermometry. Analysis of the measurements yields a value of $0.58 \pm 0.05$ for the evaporation coefficient, identical to that previously determined for pure water. These results imply that sub-saturated aqueous ammonium sulfate, which is the most abundant inorganic component of atmospheric aerosol, does not affect the vapor-liquid exchange mechanism for cloud droplets, despite reducing the saturation vapor pressure of water significantly.

\body

**Introduction:**

The vapor-liquid exchange dynamics of water underlie vital processes in biology, engineering and atmospheric science. The evaporation and condensation rates of water are particularly important in the formation of cloud particles, and are among the largest unknowns in assessing the impact of indirect aerosol effects on the radiative balance in the atmosphere (1). Model studies suggest that evaporation rates slower than 10% of the maximum rate determined by gas kinetic theory for atmospherically relevant aqueous systems would indicate kinetic control over cloud growth processes, with implications for cloud and aerosol models (2, 3). Attempts to quantify the evaporation and condensation rates of water have yielded values spanning three orders of magnitude, although the most recent values converge to a single order of magnitude (4-10). This contributes to the wide variability in cloud model predictions for the anthropogenic effect on size and number of cloud condensation nuclei (CCN) and the corresponding radiative impact on the global system (1, 3, 11, 12).

Measuring evaporation and condensation rates of liquid water is difficult due to the complex heat and mass transfer processes occurring in such experiments. The temperature of the liquid surface must be accurately determined and, in most cases, both evaporation and condensation must be properly accounted for. In addition, it has been suggested that some of the earlier measurements of these rates, which typically involved static liquid surfaces, yielded artificially low rates due to the contamination of the liquid with surface impurities (6). Such impurities may well be present in atmospheric conditions; indeed, field measurements of aerosol growth rates appear to indicate such a

slowing effect (13, 14). In our previous work, we addressed the problem of accurately modeling the heat and mass transfer processes through our measurements of the free evaporation of pure $H_2O$ and pure $D_2O$ (4, 5, 10). We also studied relative evaporation rates of isotopomers in mixtures (10, 15). In these studies of pure solutions, condensation was negligible, allowing the evaporation process to be modeled accurately and then directly related to the cooling rate of the droplets. We found that evaporation for both pure $H_2O$ and pure $D_2O$ occurred at ~ 60% of the maximum rate determined by gas kinetic theory, too fast to result in a kinetic limit to cloud droplet growth. In the present study, we take the first step towards accounting for the effects of impurities on the evaporation rate by performing similar experiments on ammonium sulfate solutions.

Ammonium sulfate was selected as a realistic model system for atmospheric inorganic aerosol due to its well-documented prevalence in the troposphere. Field studies using aerosol mass spectrometers (AMS) have revealed significant fractions of the ambient aerosol to comprise aqueous ammonium and sulfate at the surface in both urban and rural areas (16). Additionally, single-particle studies have shown that the majority of atmospheric aerosol particles are internally well-mixed and consist of approximately 50% ammonium sulfate and 50% carbonaceous components, with little altitude variation (17). Many thermodynamic studies of ammonium sulfate aerosol have shown a hysteresis in the deliquescence properties. Solid particles deliquesce at relative humidities greater than ~80%, but can remain in the aqueous phase as the relative humidity drops as low as ~35%, resulting in supersaturated solution up to approximately twice the saturation concentration before efflorescence occurs (18-20). This suggests that in the atmosphere much of the ammonium sulfate aerosol will be in the form of concentrated aqueous

solution. While there have been some measurements of the kinetics of evaporation and condensation from mixed systems including aqueous ammonium sulfate (21, 22), as well as studies of other systems, such as sodium chloride (23), few studies of the aqueous ammonium sulfate system exist (14, 24). A definitive laboratory study of evaporation kinetics from concentrated ammonium sulfate solution is needed to determine if the presence of such inorganic solutes significantly affects the gas-liquid exchange dynamics for atmospheric particles.

Most studies of evaporation or condensation report a quantity known as the evaporation coefficient ($\gamma_e$) or condensation coefficient ($\gamma_c$). The condensation coefficient is also referred to as the mass accommodation coefficient or simply the accommodation coefficient ($\alpha_m$). All of these quantities are equal and are defined via the Hertz-Knudsen equation, which is a formulation of the maximum theoretical condensation rate for a given substance derived from kinetic gas theory (6):

$$J_c = \alpha_m \frac{p}{\sqrt{2\pi mkT}} . \tag{1}$$

Here $J_c$ is the condensation rate, $p$ is the vapor pressure above the liquid surface, $m$ is the molecular mass of the substance, $k$ is the Boltzmann constant, and $T$ is the temperature. The accommodation coefficient $\alpha_m$ is a quantity ranging from zero to one; a unity value implies that condensation occurs at the maximum theoretical rate, with lower values implying some kinetic limit to the condensation rate.

At equilibrium, the evaporation and condensation rates are equal, so the evaporation rate can be expressed as:

$$J_e = \gamma_e \frac{p_{sat}}{\sqrt{2\pi mkT}}, \tag{2}$$

Here $p_{sat}$ is the equilibrium vapor pressure, and the accommodation coefficient has been replaced by the evaporation coefficient $\gamma_e$. While Equation (1) can only be used to formulate the condensation rate when the vapor exhibits a Maxwell distribution of velocities (which will not apply in non-equilibrium situations with low vapor pressures), Equation (2) can be used to formulate the evaporation rate even in non-equilibrium systems because the activity of the liquid is unchanged.

Our previous measurements utilized liquid microjets to form droplet streams in vacuum with radii in the range of 6 – 7.5 _m. This allowed the study of evaporation in the absence of condensation, significantly simplifying the experimental system. This is shown by integrating the number of collisions experienced by a single evaporating molecule as it leaves the droplet and travels an infinite distance away:

$$N_{coll}(r_0,T) = \int_{r_0}^{\infty} \frac{dr}{\lambda(r,T)} = \sqrt{2}\pi d_{coll}^2 n(r_0) r_0^2 \int_{r_0}^{\infty} \frac{dr}{r^2} = \frac{r_0}{\lambda(r_0,T)}, \tag{3}$$

Here $r_0$ is the radius of the droplet, $\lambda(r,T) = [\sqrt{2}\pi d_{coll}^2 n(r)]^{-1}$ is the mean free path of the vapor, $d_{coll}$ is the collision diameter, and $n(r)$ is the number density of the vapor. For $H_2O$, the vapor pressure at 283 K, the temperature at which our measurements began, is ~ 9 torr, corresponding to a mean free path of ~10 _m (5). Thus, molecules evaporating from droplets with radii smaller than 10 _m should experience less than one collision on average, allowing condensation to be neglected. In other words, the Knudsen number $Kn = \lambda / r_0 > 1$. We used Raman thermometry to measure the temperature of the evaporating water droplets as a function of time and modeled this cooling curve with a

simple discrete model in which $\gamma_e$ is the only adjustable parameter. The studies yielded a $\gamma_e$ value of 0.62 ± 0.09 for pure $H_2O$ (5) and 0.57 ± 0.06 for pure $D_2O$ (4). We interpreted these results and our measurements of isotope effects during evaporation (10) using a modified transition-state theory (TST) formulation (15). This formulation suggested that the energetic and entropic isotope effects cancelled, resulting in similar evaporation kinetics for the two isotopic species (4).

In extending these studies to ammonium sulfate solutions, we report the value of $\gamma_e$ as defined by Equation (2). Here, however, $p_{sat}$ is the equilibrium vapor pressure of the *solution*, rather than that of pure water. Since this vapor pressure is ~13% lower than that of pure water, the maximum theoretical evaporation rate for the solution is lower than that of pure water. Ideally, the solution in this study should be as concentrated as possible in order to simulate atmospheric conditions. The saturation limit is 3.9M at 273 K (25). The measurements presented here use 3M solutions, as more concentrated solutions resulted in frequent clogging of our _m sized orifices.

**Results:**

Raman spectra were measured for droplet radii between 8.9 and 11.55 _m. We calculate that evaporation from a droplet of 11.55 _m radius or smaller will be collision-free (i.e. $Kn > 1$) for temperatures of ~283.3 K or colder. All of the data taken in this study are below that temperature, but the liquid begins at laboratory temperature (293 K), so collisions resulting in a return flux to the liquid could play a role at very early interaction times, before the first data are taken. At 293 K $Kn = 0.54$ for an 11.55 _m radius droplet and 0.70 for an 8.9 _m radius roplet. We confirmed that these effects are unimportant by repeating our previous observations of $H_2O$ evaporation, where we used

droplets of radii less than 8 _m, on larger droplet sizes. Droplets with radii of 9.5 _m, 11.05 _m and 11.9 _m were tested, yielding $\gamma_e$ values of 0.63, 0.61 and 0.55, respectively. These are in excellent agreement with our previously measured value of 0.62 ± 0.09 for $H_2O$ (5). No systematic deviation from the model predictions were found at early interaction times for either $H_2O$ or ammonium sulfate solutions. We have previously observed such deviations to occur for pure $H_2O$ droplets of 20.3 _m radius (5), suggesting that droplets must approach this size before condensation effects become important.

Eight measurements on seven different droplet sizes were collected for the 3M ammonium sulfate solution, resulting in an average $\gamma_e$ of 0.58 ± 0.05. The variance shown is the 95% confidence interval. The droplet residence times in vacuum were between 597 _s and 1014 _s. A representative experimental cooling curve for a droplet of 9.1 _m radius is shown in Figure (1), with a model fit using a $\gamma_e$ value of 0.58. As in our previous studies, the best fit to the data is found when $\gamma_e$ does not vary with temperature. Model fits for all measurements were conducted with 20 spherical shells per droplet, sufficient to produce a numerically converged temperature field.

In general, there was more noise in the experimental cooling curves in this study compared to our work on pure liquid $H_2O$ or $D_2O$. One possible explanation is the presence of icicles. The ammonium sulfate solution formed icicles in the liquid nitrogen trap much more readily than did either pure $H_2O$ or pure $D_2O$, due to salt crystallization upon freezing. Icicles often grew into the interaction region of the laser during a measurement, despite the extended length of the liquid nitrogen trap (60 cm). The issue was most prominent for droplet streams that were not completely straight and may have

impinged the side of the trap, rather than the bottom. The trap was fitted with an icicle breaker to allow icicles to be removed during measurements, but it is possible that icicles may still have interfered slightly with the measurements (causing additional noise) by providing a surface for gas-phase collisions and possibly leading to some re-condensation of vapor onto the droplet stream.

The use of ammonium sulfate solution instead of pure $H_2O$ introduces some other potential complications as well. The spectra used for the temperature calibration exhibit two features from the ammonium ion (Figure (2)). This means that the temperature measurements are sensitive to the concentration of the solution. To ensure that no dilution occurred before each measurement, the spectrum of the droplet stream in ambient air was taken to verify that laboratory temperature was reproduced; pure $H_2O$ tests revealed that this should be true for distances less than 5 mm from the nozzle. During a typical vacuum measurement, however, the volume of the droplets is expected to decrease by up to 6% due to evaporation, implying a 6 % increase in solute concentration. While this is a small change that is not expected to affect the evaporation kinetics, it alters the Raman spectrum. We calibrated the Raman spectrum as a function of temperature for both 3 and 3.18M solutions. Derived temperatures from the spectra of liquid jets were interpolated between the values from 3M solution and from 3.18M solution based on the expected concentration increase at each experimental time point.,

**Discussion:**

The $\gamma_e$ value of 0.58 ± 0.05 found in this study suggests that the presence of ammonium sulfate does not significantly affect the evaporation mechanism of liquid

water, despite the ~13% reduction in vapor pressure. This at first seems surprising; the 3M solution used in this study contains a 9M total ion concentration, and if a hydration shell of ~4-6 water molecules is assumed then virtually every water molecule should be interacting with an ion. It is reasonable to assume that these interactions would alter the mechanism for evaporation and therefore the evaporation coefficient. Our results suggest, however, that there is remarkable similarity in the efficiencies of the evaporation and condensation processes for pure water and 3M ammonium sulfate solution. This may in part be explained by the fact that both solute ions are expected to be depleted in the surface region, limiting their effect on evaporating water molecules. Molecular dynamics (MD) simulations of ammonium sulfate solution in the interfacial region show the sulfate anion completely depleted from the interface to a depth of approximately 7 Å (26). This result is in agreement with interpretations of surface tension measurements of ammonium sulfate solution (27). The ammonium ion, however, is not completely depleted from the interfacial region in the MD simulations and exists at lower density within the upper 5 Å of the interface. Thus the ammonium ion may be expected to have some interactions with evaporating water molecules. Car-Parrinello molecular dynamics (CPMD) simulations of the solvated ammonium ion predict a first solvation shell containing four tightly bound water molecules in a tetrahedral cage, and a fifth more weakly bound and more mobile water molecule that occasionally exchanges with one of the other four (28). The radius of the solvation shell is found to be ~ 3 Å. If one estimates, from the MD results presented by Gopalakrishnan et al., that the ammonium ion concentration is ~ 15 – 20% of its bulk concentration at a depth of 3 Å from the surface, then only 7 – 11% of the water molecules in the interfacial layer are within the first solvation shell of an

ammonium ion in our 3M solution, implying that any solute effects on evaporation are unimportant.

The results of this study indicate that ammonium sulfate, even if present at highly supersaturated aqueous concentrations, is not likely to significantly affect evaporation and condensation kinetics in the atmosphere, other than by reducing the vapor pressure. Field observations, however, have shown large variation in particle growth rates, including many cases in which growth rates were significantly lower than measured values for ammonium sulfate aerosol in the laboratory (14, 34). It is likely that other atmospheric constituents, e.g. organics, can affect the liquid-vapor exchange rates of water in the atmosphere and subsequently affect cloud condensation behavior. There is currently much interest in the effects of organic aerosol on the hygroscopic behavior of atmospheric particles (13, 21, 22, 35, 36), although, to date, available kinetic information has been limited. A more recent study by Shantz et al. shows that anthropogenic aerosol in the field, consisting of ammonium sulfate and organic components, exhibits growth rates consistent with a lowering of $\gamma_e$ by over an order of magnitude relative to pure ammonium sulfate aerosol (34). The specific effects of different organic species in that study could not be determined, however. New and improved methods are needed to quantify the effect of organic surfactant films on evaporation and condensation rates in the atmosphere.

From a purely physical perspective, other inorganic solutes might be expected to alter evaporation rates more readily. Ions such as thiocyanate and perchlorate, which are expected to be strongly enhanced in concentration at the air-water interface might be expected to have large effects on $\gamma_e$ through direct interactions with evaporating water

molecules (37). Studies of perchlorate solutions are currently underway in our laboratory.

**Materials and Methods:**

*Sample Preparation:*

Samples were prepared volumetrically, using commercial anhydrous ammonium sulfate (Sigma Aldrich, ≥99%) and deionized and filtered $H_2O$ (18.2 MΩ resistivity, Milli-Q, Millipore). Solutions were then filtered through a 2 _m particle retention filter and stored in a sealed container when not in use.

*Experimental Apparatus:*

The experimental apparatus has been described in detail previously (4, 5). Briefly, a syringe pump (Teledyne ISCO Model 260D) is used to pump the sample solution through a fused silica orifice mounted on a piezoelectric ceramic. In our earlier studies, the orifice radii used were 2.5-4 _m; however, clogging issues upon running salt solutions necessitated larger orifices for this study, in the range of 4-6.5 _m diameter. The orifices were prepared from 100 _m ID fused silica tubing using a $CO_2$ laser micropipette puller (Sutter Instrument Co. Model P2000). Orifice sizes were determined via Mie scattering of a HeNe laser intersecting the liquid stream, in the same manner described previously (10). The piezoelectric ceramic allows the silica orifice to act as a Vibrating Orifice Aerosol Generator (VOAG). By driving the piezoelectric ceramic with a 20V square wave at 300 – 800 kHz, a uniform droplet stream is generated with a spread

in radius of less than 0.1 _m (38). Droplets in this study were between 8.9 and 11.55 _m in radius; sizes were calculated from the liquid flow rate and oscillation frequency (4).

The VOAG apparatus is mounted on an XYZ manipulator stage which is in turn attached to a 7 cm cubical vacuum chamber via a bellows, allowing for positioning of the droplet stream within the chamber. The vacuum chamber is pumped by a 110 L/s turbomolecular pump. The droplet stream is intercepted by the 514.5 nm line of an argon ion laser operating at <250 mW. After the laser has passed through the droplet stream, the laser light is detected on a photodiode. Droplets passing through the laser focal volume lower the signal on the photodiode, allowing for real-time monitoring of the droplet stream produced by the VOAG and ensuring that a uniform droplet stream is being generated for any given driving frequency. After the droplet stream has passed through the laser focal volume, the liquid is captured in a liquid nitrogen trap. The trap used in this study was extended compared to that used in our previous studies and was equipped with an icicle breaker. Raman scatter from the droplets is collected and filtered at 90° and sent via fiber-optic cable to a monochromator (f/6.5) with a liquid nitrogen cooled CCD detector. The OH-stretching region of the Raman spectrum of ( 2500 – 3900 $cm^{-1}$) is used to determine the temperature of the droplets via Raman thermometry with a precision of ±2 K (4, 5). First, a calibration is taken by splitting the spectrum at an arbitrary frequency and plotting natural logarithm of the ratio of the area under the spectrum before and after the split point versus inverse temperature, giving a linear relationship. Calibration spectra were taken using solutions in a constant temperature cuvette (Figure (2)) (4). The spectra show two features near 2875 $cm^{-1}$ and 3075 $cm^{-1}$ due to the ammonium ion (39). The calibration curve allows the determination of the

temperature of the droplets in vacuum from their Raman spectra. To account for increasing concentration due to evaporaton in vacuum, separate calibration curves were taken for 3M and 3.18M solution. Raman measurements were taken as a function of distance from the VOAG nozzle. Droplet stream velocity, calculated from the liquid flow rate and orifice size, is used to calculate the residence time in vacuum. The initial temperature of the droplets is the ambient temperature in the lab.

*Evaporative Cooling Model*

We determine $\gamma_e$ by relating the temperature derived from the Raman spectra to evaporation rates, under the assumption that each evaporative event results in cooling of the solution (4, 5). We infer the effect on solution temperature by calculating the heat loss from a droplet due to evaporation. The droplet is divided into concentric spherical shells, with evaporation occurring in the outermost shell. Heat is then propagated outwards from the inner shells according to the thermal diffusion equation; this ensures an accurate droplet surface temperature. Mass loss due to evaporation from the outermost shell is accounted for; all shells are resized after each time step, then the process is iterated. Using Equation (2), the cooling rate of the droplets is defined as

$$\frac{dT}{dt} = -\gamma_e A \frac{p_{sat}}{\sqrt{2\pi mkT}} \frac{\Delta H_{vap}}{C_p \rho V_s} , \tag{6}$$

where A is the surface area of the outermost shell ($= 4\pi r_0^2$), $\Delta H_{vap}$ is the enthalpy of vaporization (44.4 kJ/mol), $C_p$ is the specific heat capacity, $\rho$ is the density, and $V_s$ is the volume of the outermost shell ($= \frac{4}{3}\pi r_0^3$). For a 3M ammonium sulfate solution, a

value of 60.625 J/mol was used for $C_p$ (40). The value of $p_{sat}$ was determined by applying a water activity of 0.874 to the empirical temperature-dependent equation for vapor pressure of pure water reported by Murphy and Koop (41). The water activity was determined from the data of Tang and Munkelwitz (42) and was assumed to be invariant with temperature. The density of the solution was measured as 1.188 g/ml and was assumed to be constant with temperature. Such an assumption proved valid for our previous work on pure $H_2O$ and $D_2O$ (4, 5).

Equation (6) can be simplified to

$$\frac{dT}{dt} = -\gamma_e \frac{p_{sat}}{\sqrt{2\pi mkT}} \frac{\Delta H_{vap}}{C_p} \frac{3r_0^2}{(r_0^3 - r_1^3)\rho}, \tag{7}$$

where $r_0$ and $r_1$ are the outer and inner radii of the outermost droplet, respectively. Here $\gamma_e$ is the only adjustable parameter. Heat transfer between adjacent shells in the droplet is modeled with the thermal diffusion equation

$$\frac{dQ}{dt} = -\kappa A \frac{dT}{dr}, \tag{8}$$

where dQ/dt is the heat transferred from the inner shell to the outer shell over the duration of a time step, $\kappa = 0.532$ is the thermal conductivity (43), $A$ is the surface area of the inner shell in question, and dT/dr is the temperature difference between the two shells. The volume-averaged temperature is then calculated at each time step; this is matched to experiment by tuning $\gamma_e$. While the Raman response from liquid microdroplets has been demonstrated to be nonuniform (44), the effect is minimized when collecting Raman signal at 90 degrees, and the response becomes more uniform for droplet radii larger than 5 _m (45). In addition, since our experiment does not trap a single droplet but rather

samples a droplet stream, there is further averaging of the Raman response over the droplet volume. As a test, we matched the experimental temperatures to the average temperature of only the outermost five spherical shells, rather than the volume averaged temperature of the entire droplet, resulting in a change of only a few percent in $\gamma_e$. In light of this, we have elected to use the volume averaged temperature model output to match experiment.

The cooling model is also used to account for the change in the Raman spectra upon increasing concentration due to evaporation in vacuum. The model predicts the change in droplet size at each time step, and therefore the expected concentration increase as a function of time. The expected concentration at each of the experimental time points is used to interpolate between the temperatures produced by the 3M and 3.18M calibrations. The model is tuned by changing $\gamma_e$ until the volume-averaged temperature predicted by the model matches the interpolated derived temperatures from the Raman measurements.

**Acknowledgements:**

This work was supported by NSF ATM 0639847 and the Director, Office of Science, Office of Basic Energy Sciences, of the US Department of Energy under Contract No. DE-AC02-05CH11231. Walter S. Drisdell thanks Robert M. Onorato and Dale E. Otten for enlightening discussions.

**References:**

1. Forster P, V. Ramaswamy, P. Artaxo, T. Berntsen, R. Betts, D.W. Fahey, J. Haywood, J. Lean, D.C. Lowe, G. Myhre, J. Nganga, R. Prinn, G. Raga M S a R V D (2007) in *Climate Change 2007: The Physical Science Basis. Contribution of Working Group I to the Fourth Assessment Report of the Intergovernmental Panel on Climate Change*, ed. Solomon, S., D. Qin, M. Manning, Z. Chen, M. Marquis, K.B. Averyt, M.Tignor and H.L. Miller (Cambridge University Press, Cambridge).
2. Chuang P Y, Charlson R J, Seinfeld J H (1997) Kinetic limitations on droplet formation in clouds. *Nature* 390**:** 594-596.
3. Laaksonen A, et al. (2005) Commentary on cloud modelling and the mass accommodation coefficient of water. *Atmospheric Chemistry And Physics* 5**:** 461-464.
4. Drisdell W S, et al. (2008) Determination of the evaporation coefficient of D2O. *Atmos. Chem. Phys.* 8**:** 6699.
5. Smith J D, et al. (2006) Raman thermometry measurements of free evaporation from liquid water droplets. *Journal Of The American Chemical Society* 128**:** 12892-12898.
6. Eames I W, Marr N J, Sabir H (1997) The evaporation coefficient of water: A review. *International Journal Of Heat And Mass Transfer* 40**:** 2963-2973.
7. Marek R, Straub J (2001) Analysis of the evaporation coefficient and the condensation coefficient of water. *International Journal Of Heat And Mass Transfer* 44**:** 39-53.
8. Davidovits P, et al. (2006) Mass accommodation and chemical reactions at gas-liquid interfaces. *Chemical Reviews* 106**:** 1323-1354.
9. Zientara M, Jakubczyk D, Kolwas K, Kolwas M (2008) Temperature Dependence of the Evaporation Coefficient of Water in Air and Nitrogen under Atmospheric Pressure: Study in Water Droplets. *J. Phys. Chem. A* 112**:** 5152-5158.
10. Cappa C D, et al. (2005) Isotope fractionation of water during evaporation without condensation. *Journal Of Physical Chemistry B* 109**:** 24391-24400.
11. McComiskey A, Feingold G (2008) Quantifying Error in the Radiation Forcing of the First Aerosol Indirect Effect. *Geophysical Research Letters* 35.
12. Lohmann U, Quaas J, Kinne S, Feichter J (2007) Different approaches for constraining global climate models of the anthropogenic indirect aerosol effect. *Bulletin Of The American Meteorological Society* 88**:** 243-249.
13. Feingold G, Chuang P Y (2002) Analysis of the influence of film-forming compounds on droplet growth: Implications for cloud microphysical processes and climate. *Journal Of The Atmospheric Sciences* 59**:** 2006-2018.
14. Ruehl C R, Chuang P Y, Nenes A (2008) How quickly do cloud droplets form on atmospheric particles? *Atmos. Chem. Phys.* 8**:** 1043.
15. Cappa C D, et al. (2007) Interpreting the H/D isotope fractionation of liquid water during evaporation without condensation. *Journal Of Physical Chemistry C* 111**:** 7011-7020.
16. Zhang Q, et al. (2007) Ubiquity and dominance of oxygenated species in organic aerosols in anthropogenically-influenced Northern Hemisphere midlatitudes. *Geophysical Research Letters* 34.

17. Murphy D M, et al. (2006) Single-particle mass spectrometry of tropospheric aerosol particles. *J. Geophys. Res.* 111.
18. Tang I N, Munkelwitz H R (1993) Composition And Temperature-Dependence Of The Deliquescence Properties Of Hygroscopic Aerosols. *Atmospheric Environment Part A-General Topics* 27**:** 467-473.
19. Onasch T B, et al. (1999) Infrared spectroscopic study of the deliquescence and efflorescence of ammonium sulfate aerosol as a function of temperature. *Journal Of Geophysical Research-Atmospheres* 104**:** 21317-21326.
20. Cziczo D J, Abbatt J P D (1999) Deliquescence, efflorescence, and supercooling of ammonium sulfate aerosols at low temperature: Implications for cirrus cloud formation and aerosol phase in the atmosphere. *Journal Of Geophysical Research-Atmospheres* 104**:** 13781-13790.
21. Sjogren S, et al. (2007) Hygroscopic growth and water uptake kinetics of two-phase aerosol particles consisting of ammonium sulfate, adipic and humic acid mixtures. *Journal Of Aerosol Science* 38**:** 157-171.
22. Garland R M, et al. (2005) Impact of palmitic acid coating on the water uptake and loss of ammonium sulfate particles. *Atmospheric Chemistry And Physics* 5**:** 1951-1961.
23. Richardson C B, Lin H B, McGraw R, Tang I N (1986) Growth-Rate Measurements For Single Suspended Droplets Using The Optical Resonance Method. *Aerosol Science And Technology* 5**:** 103-112.
24. Rose D, et al. (2008) Calibration and measurement uncertainties of a continuous-flow cloud condensation nuclei counter (DMT-CCNC): CCN activation of ammonium sulfate and sodium chloride aerosol particles in theory and experiment. *Atmospheric Chemistry And Physics* 8**:** 1153-1179.
25. Robertson J (1985) Densities of aqueous solutions of inorganic substances by O. Sohnel and P. Novotny. *Acta Crystallographica Section B* 41**:** 208.
26. Gopalakrishnan S, Jungwirth P, Tobias D J, Allen H C (2005) Air-liquid interfaces of aqueous solutions containing ammonium and sulfate: Spectroscopic and molecular dynamics studies. *Journal Of Physical Chemistry B* 109**:** 8861-8872.
27. Pegram L M, Record M T (2007) Hofmeister salt effects on surface tension arise from partitioning of anions and cations between bulk water and the air-water interface. *Journal Of Physical Chemistry B* 111**:** 5411-5417.
28. Bruge F, Bernasconi M, Parrinello M (1999) Ab initio simulation of rotational dynamics of solvated ammonium ion in water. *Journal Of The American Chemical Society* 121**:** 10883-10888.
29. Pudzianowski A T (1995) Mp2/6-311++G(D,P) Study Of 10 Ionic Hydrogen-Bonded Binary-Systems - Structures, Normal-Modes, Thermodynamics, And Counterpoise Energies. *Journal Of Chemical Physics* 102**:** 8029-8039.
30. Bruge F, Bernasconi M, Parrinello M (1999) Density-functional study of hydration of ammonium in water clusters. *Journal Of Chemical Physics* 110**:** 4734-4736.
31. Hofmeister F (1888) Zur Lehre von der Wirkung der Salze. *Naunyn-Schmiedeberg's Archives of Pharmacology* 24**:** 247.

32. Collins K D, Washabaugh M W (1985) The Hofmeister Effect And The Behavior Of Water At Interfaces. *Quarterly Reviews Of Biophysics* 18**:** 323-422.
33. Cacace M G, Landau E M, Ramsden J J (1997) The Hofmeister series: salt and solvent effects on interfacial phenomena. *Quarterly Reviews Of Biophysics* 30**:** 241-277.
34. Shantz N C, et al. (2009) Slower CCN growth kinetics of anthropogenic aerosol compared to biogenic aerosol observed at a rural site. *Atmos. Chem. Phys. Discuss.* 9**:** 13775.
35. Abbatt J P D, Broekhuizen K, Kumal P P (2005) Cloud condensation nucleus activity of internally mixed ammonium sulfate/organic acid aerosol particles. *Atmospheric Environment* 39**:** 4767-4778.
36. Shantz N C, Leaitch W R, Caffrey P F (2003) Effect of organics of low solubility on the growth rate of cloud droplets. *Journal Of Geophysical Research-Atmospheres* 108.
37. Petersen P B, Saykally R J, Mucha M, Jungwirth P (2005) Enhanced concentration of polarizable anions at the liquid water surface: SHG spectroscopy and MD simulations of sodium thiocyanide. *Journal Of Physical Chemistry B* 109**:** 10915-10921.
38. Sayer R M, Gatherer R D B, Gilham R J J, Reid J P (2003) Determination and validation of water droplet size distributions probed by cavity enhanced Raman scattering. *Physical Chemistry Chemical Physics* 5**:** 3732-3739.
39. Fawcett V, Long D A, Sankaranarayanan V N (1975) Study Of Internal Frequency Region (400-4000cm-1) Of Raman-Spectrum Of A Single-Crystal Of Sodium Ammonium-Sulfate Dihydrate, Nanh4so4.2h2o Over Temperature-Range 293-87k. *Journal Of Raman Spectroscopy* 3**:** 217-228.
40. Roth K, Wolf U, Wolf G (1997) A simple method for modelling and prediction of the specific heat and density of aqueous electrolyte solutions. *Calphad-Computer Coupling Of Phase Diagrams And Thermochemistry* 21**:** 475-481.
41. Murphy D M, Koop T (2005) Review of the vapour pressures of ice and supercooled water for atmospheric applications. *Quarterly Journal Of The Royal Meteorological Society* 131**:** 1539-1565.
42. Tang I N, Munkelwitz H R (1994) Water Activities, Densities, And Refractive-Indexes Of Aqueous Sulfates And Sodium-Nitrate Droplets Of Atmospheric Importance. *Journal Of Geophysical Research-Atmospheres* 99**:** 18801-18808.
43. Riedel L (1951) Die Wärmeleitfähigkeit von wäßrigen Lösungen starker Elektrolyte. *Chemie Ingenieur Technik - CIT* 23**:** 59-64.
44. Schweiger G (1990) Raman-Scattering On Single Aerosol-Particles And On Flowing Aerosols - A Review. *Journal Of Aerosol Science* 21**:** 483-509.
45. Reid J P, Mitchem L (2006) Laser probing of single-aerosoldroplet dynamics. *Annual Review Of Physical Chemistry* 57**:** 245-271.

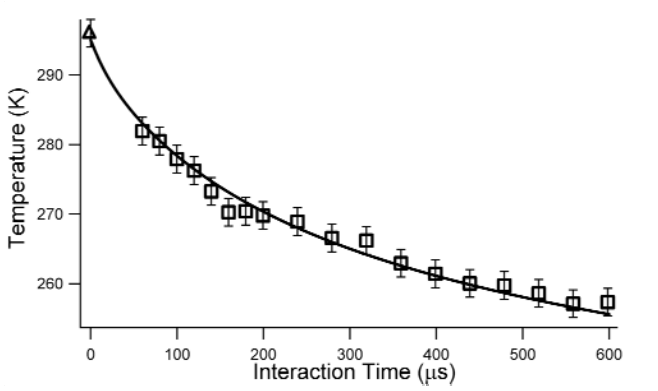


**Figure 1:** Experimental data for droplets of 9.1 _m diameter, consisting of 19 temperature values. The triangle represents the measurement of the initial droplet temperature taken in ambient air. The squares are data from the droplet in vacuum. Error bars are ± 2 K, and provide an estimate of the precision of determining the temperature from the Raman spectra. The solid line is the model fit, corresponding to $\gamma_e$ = 0.58. Deviation in the experimental data from the model fit at ~ 160 _s and ~315 _s may be due to the presence of icicles in the vacuum chamber when the corresponding spectra were collected.

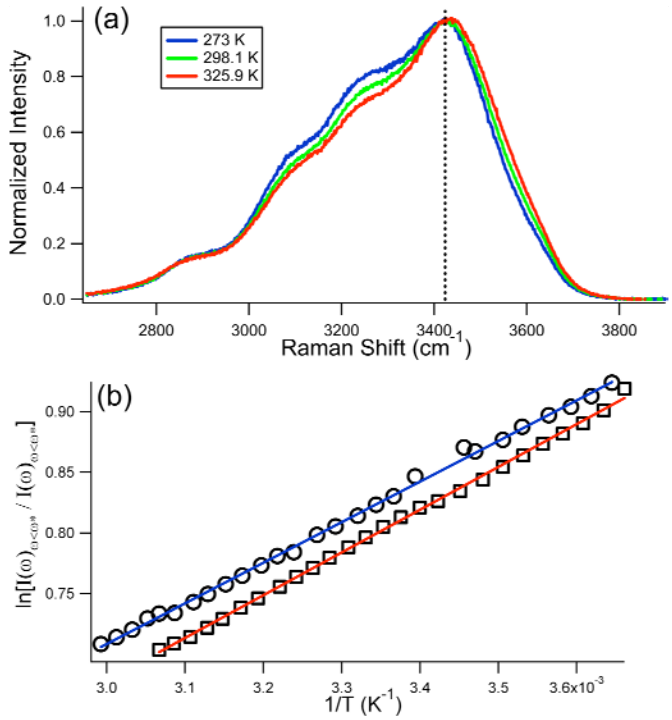


**Figure 2:** Selected spectra of 3M ammonium sulfate solution (a) collected at 273 K, 298.1 K, and 325.9 K and used for temperature calibration. The features at ~2875 $cm^{-1}$ and ~3075 $cm^{-1}$ are due to the ammonium ion. The dotted black line represents the frequency _* = 3424 $cm^{-1}$ at which the spectra were split; the natural log of the ratio of the area under the spectrum below this frequency to the area under the spectrum above this frequency shows a linear relationship when plotted versus 1/T, as shown in (b). The squares in (b) represent the full calibration curve for 3M ammonium sulfate, featuring 26 spectra collected at temperatures between 273 K and 325.9 K. The red line is the linear fit ($R^2$ = 0.9988). The circles represent the full calibration curve for 3.18M ammonium sulfate, featuring 27 spectra at temperatures between 274.35 K and 334.15 K. The blue line is the linear fit ($R^2$ = 0.9981). Experimental temperatures are determined by interpolating between these two curves based on the expected concentration at each time

point. The choice of the frequency _* is arbitrary; the frequency chosen is convenient for alternating between calibration curves for ammonium sulfate solution and pure water.